THE JOURNAL OF BIOLOGICAL CHEMISTRY VOL. 289, NO. 22, pp. 15867–15879, May 30, 2014

Molecular Basis of the General Base Catalysis of an α/β-Hydrolase Catalytic Triad*

Received for publication, November 22, 2013, and in revised form, March 22, 2014 Published, JBC Papers in Press, April 15, 2014, DOI 10.1074/jbc.M113.535641

Yueru Sun[‡§], **Shuhui Yin**[‡§], **Yitao Feng**[‡§], **Jie Li**[¶], **Jiahai Zhou**[¶], **Changdong Liu**[§‖], **Guang Zhu**[§‖], **and Zhihong Guo**[‡§1]

From the [‡]*Department of Chemistry,* [‖]*Division of Life Sciences, and* [§]*State Key Laboratory of Molecular Neuroscience, The Hong Kong University of Science and Technology, Clear Water Bay, Kowloon, Hong Kong Special Administrative Region (SAR), China and* [¶]*State Key Laboratory of Bio-organic and Natural Products Chemistry, Shanghai Institute of Organic Chemistry, Chinese Academy of Sciences, 345 Lingling Road, Shanghai 200032, China*

Background: The α/β-hydrolase MenH uses its Ser-His-Asp triad as a specific general basis with a poorly understood mechanism.
Results: An open-closed conformational change is identified in the enzyme catalysis.
Conclusion: The conformational change controls the formation and reactivity of the catalytic triad.
Significance: The catalytic versatility of the Ser-His-Asp triad is expanded by the open-closed structural change.

The serine-histidine-aspartate triad is well known for its covalent, nucleophilic catalysis in a diverse array of enzymatic transformations. Here we show that its nucleophilicity is shielded and its catalytic role is limited to being a specific general base by an open-closed conformational change in the catalysis of (1*R*,6*R*)-2-succinyl-6-hydroxy-2,4-cyclohexadiene-1-carboxylate synthase (or MenH), a typical α/β-hydrolase fold enzyme in the vitamin K biosynthetic pathway. This enzyme is found to adopt an open conformation without a functional triad in its ligand-free form and a closed conformation with a fully functional catalytic triad in the presence of its reaction product. The open-to-closed conformational transition involves movement of half of the α-helical cap domain, which causes extensive structural changes in the α/β-domain and forces the side chain of the triad histidine to adopt an energetically disfavored *gauche* conformation to form the functional triad. NMR analysis shows that the inactive open conformation without a triad prevails in ligand-free solution and is converted to the closed conformation with a properly formed triad by the reaction product. Mutation of the residues crucial to this open-closed transition either greatly decreases or completely eliminates the enzyme activity, supporting an important catalytic role for the structural change. These findings suggest that the open-closed conformational change tightly couples formation of the catalytic triad to substrate binding to enhance the substrate specificities and simultaneously shield the nucleophilicity of the triad, thus allowing it to expand its catalytic power beyond the nucleophilic catalysis.

The serine (Ser)-histidine (His)-aspartate (Asp) triad is a well known catalytic motif that is utilized in catalysis of a diverse array of chemical transformations by a large number of enzymes. One group of these triad-dependent enzymes includes numerous hydrolytic enzymes in the trypsin and subtilisin families of serine peptidases that cleave C–N bonds in peptide substrates (1). Another group of enzymes utilizing this triad or its variants are members of the α/β-hydrolase fold superfamily that catalyze cleavage of C–O, C–S, C–C, or C–halogen bonds in structurally diverse metabolites or even cofactor-independent haloperoxidation and dioxygenation of electron-rich substrates (2, 3). Commensurate with their functional diversity, these enzymes display vast structural diversity in size, structure fold, and three-dimensional architecture. However, they converge to form the conserved triad and the associated oxyanion hole as a stable, integrative catalytic unit from distal residues, which are arranged in one enantiomeric configuration in α/β-hydrolase fold enzymes and in another configuration in members of the trypsin and subtilisin families (3). Besides this structural conservation, a majority of these enzymes use the triad to catalyze the diverse chemical transformations via a similar nucleophilic mechanism, which is characterized by formation of a covalent enzyme adduct involving nucleophilic addition of the triad serine to the substrate (3, 4).

Besides the traditional nucleophilic mechanism of catalysis, the Ser-His-Asp triad has also been proposed to play the role of a simple general base in the catalysis of some α/β-hydrolases. In the catalysis of cyanohydrin lyases, the triad is postulated to deprotonate hydrogen cyanide for addition to aldehydes and ketones (5, 6) despite the fact that this triad is able to form a covalent complex with trichloroacetaldehyde through nucleophilic addition (6). A similar general base role was also proposed for the triad of C–C bond hydrolases (7–9), which are involved in the degradation pathways of aromatic compounds. However, recent investigations have shown that the C–C bond hydrolase BphD adopts the traditional covalent, nucleophilic mechanism of catalysis because of the finding of an acyl-enzyme intermediate (10, 11). Noticeably, the triad serine in these enzymes has been demonstrated to exhibit nucleophilic reactivity (5, 12). In addition, a nucleophilic mechanism of catalysis

* This work was supported in part by Grants GRF601413, GRF601209, and RPC11SC16 from the Research Grants Council of the Hong Kong Special Administrative Region government (to Z. G.) and by National Natural Science Foundation of China Grant NSFC 11079051 (to J. Z.).
The atomic coordinates and structure factors (codes 4MXD, 4MYD, and 4MYS) have been deposited in the Protein Data Bank (http://wwpdb.org/).
[1] To whom correspondence should be addressed: Dept. of Chemistry, The Hong Kong University of Science and Technology, Clear Water Bay, Kowloon, Hong Kong SAR, China. Tel.: 852-23587352; Fax: 852-23581594; E-mail: chguo@ust.hk.

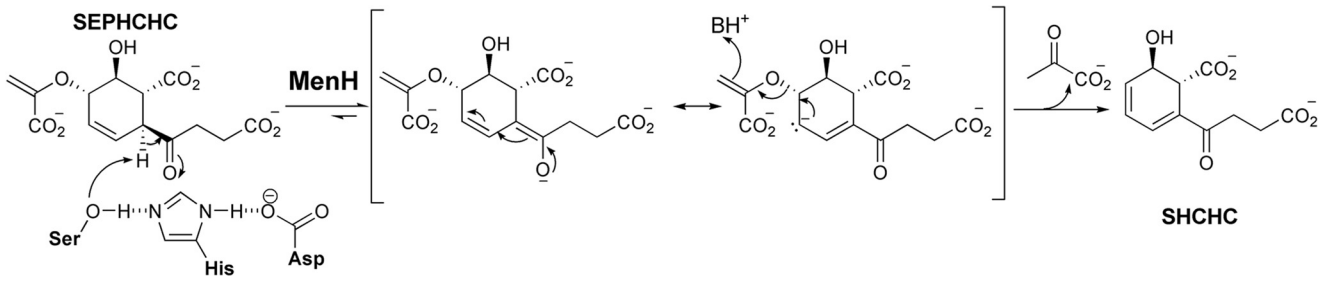

FIGURE 1. **The proposed general basis catalysis of 2,5-elimination of pyruvate by the Ser-His-Asp triad of the vitamin K biosynthetic enzyme MenH.**

is able to explain the reactions catalyzed by these enzymes equally well as the general base mechanism of catalysis (10, 13).

Recently, the vitamin K biosynthetic enzyme (1*R*,6*R*)-2-succinyl-6-hydroxy-2,4-cyclohexadiene-1-carboxylate (SHCHC)[2] synthase (MenH) has been shown to use its Ser-His-Asp triad as a general base. This enzyme is also a typical α/β-hydrolase fold enzyme and is responsible for 2,5-elimination of pyruvate from (1*R*,2*S*,5*S*,6*S*)-2-succinyl-5-enolpyruvyl-6-hydroxy-3-cyclohexene-1-carboxylate (SEPHCHC) to form SHCHC (14), which is a chemical conversion difficult to adopt a nucleophilic mechanism of catalysis commonly utilized by serine proteases and other α/β-fold hydrolases. The MenH catalytic triad most likely catalyzes simple abstraction of a proton from the α-carbon of the succinyl carbonyl group of the substrate to form an enolate intermediate that subsequently undergoes elimination of the enolpyruvyl group in an E1cb mechanism (Fig. 1) (15). This distinctive MenH catalytic mechanism demonstrates that the classical Ser-His-Asp triad is indeed capable of new catalytic chemistry.

Despite its unique mechanism of catalysis, the MenH triad is not found to be structurally different from that of other triad-utilizing enzymes (Refs. 14, 17, and 18 and Protein Data Bank code 1R3D). In addition, mutational studies found that the MenH catalytic triad contributes to rate enhancement of at least 10^6-fold to the catalysis of the enzyme (14), similar to the catalytic contribution of the triads of serine proteases. At present, it is not clear why the structurally similar triad plays the role of a catalytic base in MenH catalysis but a nucleophile in catalysis of other triad-dependent enzymes. To further understand the catalytic mechanism of MenH, we determined the crystal structure of the enzyme with and without its products. We found that formation of the catalytic triad is subject to control by an open-closed conformational change. This finding not only provides new insights into the MenH catalytic mechanism but also reveals a new mechanism for control and modulation of reactivity of the catalytic triad.

EXPERIMENTAL PROCEDURES

Protein Expression and Purification—The expression constructs of the mutants of *Escherichia coli* MenH, including V152A, V152G, F153A, Y148F, Y148A, V152G/F153A, and W147A/Y148A, were generated with a QuikChange site-directed mutagenesis kit (Stratagene). All mutants were sequenced to ensure that only the expected mutations had been incorporated into the amplified DNA. The wild-type MenH and its mutants were expressed and purified according to a procedure reported previously (15). Briefly, the expression plasmid for a target protein was transformed into *E. coli* strain BL21(DE3), and the resulting recombinant cells were grown in Luria broth (LB) containing 100 μg/ml ampicillin. For expression of ^{15}N-labeled MenH, the cells were grown in M9 minimum medium containing 1g/liter [^{15}N]NH_4Cl and 100 μg/ml ampicillin. Overexpression of all proteins was induced using 0.2 mM isopropyl 1-thio-β-D-galactopyranoside for 16 h at 18 °C. The recombinant proteins were purified to greater than 95% purity as indicated by SDS-PAGE via Ni^{2+}-chelating column chromatography followed by size exclusion chromatography. The purified unlabeled proteins were concentrated and stored in 25 mM Tris-HCl, pH 8.0 and 10% glycerol for crystallization or activity assays, whereas the labeled protein was stored in 50 mM sodium phosphate buffer containing 50 mM NaCl and 10% glycerol at pH 7.4. Protein concentration was estimated using a Coomassie Blue protein assay kit (Pierce).

Product Preparation and Enzyme Activity Assay—The reaction product of MenH, SHCHC, was prepared using a chemoenzymatic method described previously (14) from chorismic acid and 2-ketoglutarate using recombinant EntC (19, 20), MenD (21), MenC (21), and MenH (14). Typically, a mixture of 12.5 mM chorismate, 50 mM 2-ketoglutarate, 75 μM thiamine diphosphate, and 7.5 mM $MgSO_4$ was incubated with 30 μM EntC, 30 μM MenD, and 15 μM MenH in 200 mM sodium phosphate buffer at 32 °C for 3 h. The resulting SHCHC solution was then purified by HPLC using an isocratic elution with aqueous solution containing 1% formic acid. The enzyme substrate SEPHCHC was synthesized similarly in the absence of MenH (22). Chorismic acid was extracted from the metabolites of an engineered bacterial strain (23).

The assay for the SHCHC synthase activity of MenH has been described previously (14). Briefly, the reactions were carried out in 50 mM sodium phosphate buffer at pH 7.0 containing the SEPHCHC substrate at varied concentrations. MenH and its mutants were then added to the mixture to initiate the reaction. Production of SHCHC was monitored in real time by the increase in absorbance at 290 nm.

NMR Experiments—One-dimension NMR spectra were acquired on a Varian UNITY Inova 500-MHz NMR spectrometer equipped with an actively *z*-gradient-shielded triple resonance probe where the water signal was suppressed using the WATERGATE sequence. For each spectrum, 1024 scans were

[2] The abbreviations used are: SHCHC, (1*R*,6*R*)-2-succinyl-6-hydroxy-2,4-cyclohexadiene-1-carboxylate; MenH, (1*R*,6*R*)-2-succinyl-6-hydroxy-2,4-cyclohexadiene-1-carboxylate synthase; SEPHCHC, (1*R*,2*S*,5*S*,6*S*)-2-succinyl-5-enolpyruvyl-6-hydroxy-3-cyclohexene-1-carboxylate; r.m.s.d., root mean square difference.

acquired consisting of 128,000 data points with a spectral width of 35 ppm at 4 °C. The concentration of MenH or the H232A mutant was fixed at 0.33 mM, and SHCHC was titrated into the MenH solution to a concentration of 0.165, 0.33, and 0.66 mM. As a control, one-dimension proton NMR was collected for 0.36 mM SHCHC alone. To determine which of the protons at $\delta_H = 19.10$ and 14.16 ppm is hydrogen-bonded to the imidazole side chain of His^{232}, a mixture of 0.40 mM ^{15}N-labeled MenH and 0.80 mM SHCHC was used for analysis by heteronuclear single quantum coherence spectroscopy. However, no cross-peaks were found probably because of the weak ^{15}N signals.

Fluorometric Determination of Binding Affinity—The dissociation constant (K_D) for binding of the SHCHC ligand by MenH or its H232A mutant was determined by the ligand-dependent quenching of tryptophan fluorescence with a PerkinElmer Life Sciences Model LS-55 luminescence spectrometer. Specifically, the SHCHC ligand was titrated into the solution of MenH or the H232A mutant at 2.0 μM in the 25 mM Tris-HCl buffer, pH 8.0. The tryptophan fluorophore was excited at 280 nm, and its emission (F) at 340 nm was recorded. The dissociation constant was determined by the least square fitting of the fluorescence-[SHCHC] curves according to the equation $F/F_0 = K_D/(K_D + [\text{SHCHC}])$ where F_0 is the tryptophan fluorescence of the protein in the absence of any ligands.

Stopped-flow Kinetics—Rapid kinetic measurements of either UV-visible absorption or fluorescence emission were performed on an Applied Photophysics SX.18MV-R stopped-flow reaction analyzer mounted with an Applied Photophysics spectral kinetic monochromator. In pre-steady state kinetic measurements, 50-μl aliquots of MenH at 2.0 μM were mixed with an equal volume of SEPHCHC solution at concentrations varying from 5.0 to 240 μM. The release of the SHCHC product was monitored at 290 nm for a total of 200 ms with a 1-ms dead time. In the kinetic measurement of SHCHC binding, 50-μl aliquots of MenH at 1.0 μM were mixed with an equal volume of SHCHC at concentrations varying from 0 to 360 μM. Quenching of the tryptophan fluorescence emission at 340 nm was determined over a period of 200 ms as a change of fluorescence voltage (photomultiplier tube voltage) using a 305-nm high pass filter with a monochromatic excitation wavelength of 280 nm. The buffer used in the stopped-flow experiments was 0.20 M phosphate buffer at pH 7.0. The slit width of the monochromator source was set to 8 nm in all experiments.

Crystallization—Initial screening of crystallization conditions for ligand-free MenH and MenH in complex with SHCHC was performed using hanging drop vapor diffusion with a range of screen kits (Hampton Research) at 293 K. The concentrations of MenH and SHCHC were 10 mg/ml and 2 mM, respectively. The protein solution was mixed with the reservoir solution in a 1:1 ratio in these screening trials. Small ellipsoid and rhombohedral crystals were obtained within 1 week under the same conditions for both the complex and the ligand-free protein. After several rounds of optimization, the longest dimension of the crystals reached about 100 μm. However, neither the complex nor the ligand-free protein crystals diffracted to a high resolution on an in-house x-ray diffractometer. After optimization via additive screens using the Crystal Screen kit and Crystal Screen II kit (Hampton Research), cuboid-shaped crystals of ligand-free MenH were observed in solution containing 0.2 M Li_2SO_4, 0.1 M Tris buffer, pH 9.0, 30% (v/v) glycerol, and 17% PEG 3350 with a dimension of 300 × 300 × 200 μm. Large, rod-shaped crystals (500 μm for the longest dimension) of the MenH complex were obtained when the initial screens were rechecked 2 months later in solution containing 1.6 M sodium/potassium phosphate, pH 6.9. The ternary complex was crystallized under the same conditions as for the binary complex with the addition of 2 mM pyruvate. The crystals were mounted and soaked in cryoprotectant containing 20% glycerol in the mother liquor and then flash frozen in liquid N_2.

Data Collection, Processing, and Structure Solution—X-ray diffraction data were collected for the crystals of ligand-free MenH and the complexes at beamline BL17U at Shanghai Synchrotron Radiation Facility with an ADSC Quantum 315R charge-coupled device detector. Diffraction images were indexed, integrated, and scaled using HKL2000 (24). The ligand-free MenH structure was solved by molecular replacement with Phaser (25) in the CCP4 suite (26) using the structure of *Vibrio cholerae* MenH (Protein Data Bank code 1R3D) as the search model. The initial electron density map indicated that one MenH polypeptide chain was correctly located in the asymmetric unit in space group $P3_12_1$. The model was then extended via automatic model building using the program ARP/wARP (27) and then further built manually using Coot (28) followed by refinement using REFMAC (29) and PHENIX (30). The overall quality of the structural model was assessed by PROCHECK (31) and MolProbity (32). Data collection and refinement statistics are summarized in Table 1.

Based on the diffraction patterns, the MenH-SHCHC complex crystal is in the $P3_12_1$ space group. The crystal structure solved by molecular replacement with Phaser using the ligand-free MenH structure as the search model contained a high solvent content of 66.1% with one-third of the crystal volume occupied by non-interpretable electron densities. Although the unit cell contains MenH molecules with very well defined electron densities, this structure did not appear to be a correct solution. The diffraction data set was then reindexed to the $P3_1$ space group for structural determination by molecular replacement using Phaser and BALBES (33). The resulting structure contained two well defined MenH molecules in the asymmetric unit, which also contained uninterpreted electron densities in one-third of its volume. A third MenH molecule was successfully generated in the asymmetric unit after model building by OASIS (34) albeit with poor and disconnected electron densities. By applying the merohedral twin law (h, $-h-k$, $-l$), the model was eventually refined by Phenix.refine to a high resolution with $R_{work}/R_{free} = 0.13/0.15$. However, the actual R_{work}/R_{free} was found to be 0.23/0.25 in the validation process, indicative of the absence of twinning in the crystal. Examination of the reflection images and the self-rotation function found that the crystal likely had an order-disorder structure (35, 36). The diffused electron densities of the third MenH chain in the middle of the asymmetric unit in the $P3_1$ space group were then interpreted as two overlapping MenH chains in a 1:1 ratio that were related by a 2-fold axis. A "statistical" 2_1 axis is generated by the two overlapping MenH chains so that the symmetry of the crystal is $P3_12_1$. The structure was finally solved with $R_{work}/$

R_{free} = 0.13/0.17. Restraints of SHCHC were generated and refined using eLBOW (37). The ternary complex crystal also had an order-disorder structure and was similarly solved. Data collection and refinement statistics are summarized in Table 1.

Structural Analysis and Sequence Alignment—Sequence was analyzed with ClustalW2.0 (38). PyMOL was used in the structural analysis and generation of all graphics (39). PISA was used to analyze the protein interfaces (40), and CASTp was used to identify the binding cavities in the protein structures and to calculate the volume of the active site cavity (41).

RESULTS

Overall Structure—The ligand-free MenH, MenH-SHCHC, and MenH-SHCHC-pyruvate crystal structures were determined and refined to a resolution of 1.45, 1.37, and 1.42 Å, respectively. The asymmetric unit of the ligand-free MenH crystal contains one molecule that binds one sulfate ion and one chloride ion in close proximity in the active site. In comparison, the asymmetric unit of the binary or the ternary complex crystal structure contains three protein molecules of which two bind one or both small molecule ligands and the third in the middle is present in two C2-symmetric conformations in a 1:1 ratio without any ligands. The electron densities of the SHCHC and pyruvate ligands are very well defined with 100% occupancy for all atoms in the MenH-SHCHC and MenH-SHCHC-pyruvate complexes. The MenH molecules in the complexes are essentially identical with a root mean square difference (r.m.s.d.) of $<$0.25 Å over all 252 Cα atoms but are different from the molecule in the ligand-free protein crystal with a 12.2-Å r.m.s.d.

All the MenH molecules are composed of an α-helical cap domain and a typical α/β-hydrolase fold domain (Fig. 2*A*). The α/β-domain contains seven β-strands (β2 to β8) in the central β-pleated sheet flanked by helices (αA to αF) on both sides; it is missing the β1 strand of the canonical α/β-hydrolase fold (42). It also contains an additional 3_{10}-helix (residues 51–53) in the β4-to-αB loop and an additional short helix (αF′; residues 239–251) at the αF N terminus, both of which are absent in the canonical α/β-hydrolase fold. The α-helical cap domain is inserted in the loop connecting β6 to αD and consists of four long α-helices (α1 to α4) and two short 3_{10}-helices (α2′ and α4′) connected to the C termini of α2 and α4, respectively.

Open and Closed Conformations—Analysis of the electrostatic potential surface with APBS (43) revealed a major difference between the structures of ligand-free MenH and MenH in complex with one or both products. As shown in Fig. 2*B*, the positively charged crevice corresponds to the active site cavity formed between the helical cap domain and the α/β-domain and is significantly larger and wider in the ligand-free MenH structure than in all three molecules in the asymmetric units of the complex structures containing SHCHC (shown in Fig. 2*B*) or both SHCHC and pyruvate (not shown), including the central molecule without any ligands. Using CASTp for analysis (41), the volume of the cavity was calculated to be 1662 Å^3 in ligand-free MenH and 1013 Å^3 in the MenH-SHCHC complex, indicating a reduction of ~650 Å^3 in size upon binding of the product. This drastic change shows that MenH is in an open conformation in the ligand-free protein structure and is in a closed conformation when complexed with the ligands.

The catalytic triad is not formed in the open conformation. As shown in Fig. 2*C*, the side chains of the three triad residues Ser^{86}, His^{232}, and Asp^{210} are well separated without direct hydrogen bonding connections. The side chain of His^{232} exists in two rotamers, RT1 and RT2, of which the former is present with ~30% of the electron density in an energetically disfavored *gauche* conformation, and the latter possesses ~70% of the electron densities in an energetically favored *trans* conformation. The two nitrogen atoms in the RT1 imidazole side chain were assigned to avoid clash with the bound water molecule, which would occur after a 180° flip of the imidazole ring. Neither RT1 nor RT2 of His^{232} takes a position to interact directly with either Ser^{86} or Asp^{210}. Consequently, the open conformation of MenH is inactive without a functional catalytic triad.

In contrast, a functional catalytic triad is readily found in the closed MenH conformation with strong hydrogen bonds directly connecting Ser^{86}, His^{232}, and Asp^{210} (Fig. 2*C*), demonstrating that the closed state of MenH is active. This functional triad is found in all molecules with or without the product ligands in the asymmetric units of both the binary and ternary complex structures. It is also found in the three reported MenH structures without any product ligands (Refs. 16 and 17 and Protein Data Bank code 1R3D), indicating that they are also in the active closed conformation. Indeed, the ligand-free MenH structure from *E. coli* (Protein Data Bank code 4GDM) is superimposable with the closed structure in the MenH-SHCHC complex with an r.m.s.d. of 0.35 Å over all 252 Cα atoms. It is clear from this comparison that *E. coli* MenH exists in two structurally distinct forms in the absence of ligands of which one is the "open" structure determined in this study and the other is the previously determined "closed" conformation (18).

Open-to-closed Conformational Change—The open-closed structural difference at the MenH active site is a result of global conformational change. From a superposition of the open and closed conformations (Fig. 3*A*), a significant change is identified in the reorientation of about one-half of the cap domain consisting of α2, α2′, α3, and the connecting loops (Fig. 3*B*). This orientation change is responsible for the significant shrinkage of the active site cavity in the closed conformation (Fig. 2*B*) because the reoriented structure constitutes a large part of the active site. It also enables extensive interaction of the protein with the SHCHC ligand, including the hydrogen bonds between the SHCHC succinyl carboxylate and Arg^{168} (mediated by water), Trp^{147}, and Tyr^{148} and the hydrophobic contacts between the ligand and Trp^{147}, Val^{152}, and Phe^{153} (Fig. 3*D*). These new interactions significantly stabilize the closed conformation and may even induce its formation.

The hinged movement in the cap domain leads to a downward shift of the 3_{10}-helix α2′ by 2.3 Å toward the α/β-domain. As a result, the hydrophobic side chain of Val^{152} in the α-helix, which packs against the imidazole ring of His^{232} RT1 rotamer in the open conformation, is dislocated to pack against the His^{232} imidazole ring of the functional catalytic triad in the closed conformation, which corresponds to the position of His^{232} RT2 rotamer in the open conformation. In the meantime, the bulky side chain of the adjacent Phe^{153} is moved into the position of the imidazole ring in the RT1 rotamer of His^{232} in the open conformation, forcing the triad residue to adopt the energeti-

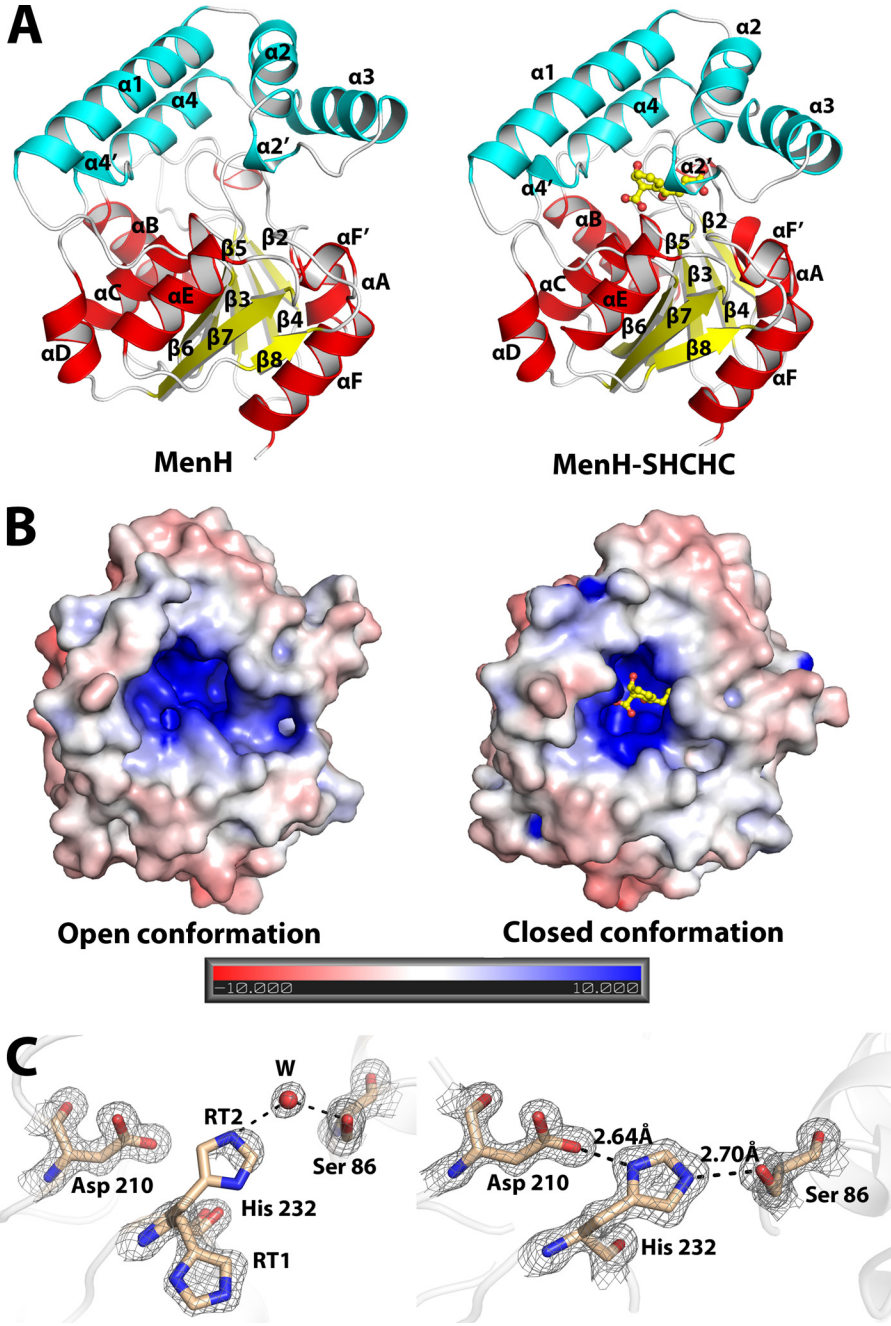

FIGURE 2. **Crystal structures of MenH in the open and closed conformations.** *A*, schematic representation of the structures. *B*, electrostatic potential surface of the structures. *C*, spatial arrangement of the triad residues Ser^{86}, Asp^{210}, and His^{232} in stick representation. In all panels, the *left* structure belongs to ligand-free MenH in the open conformation, and the *right* structure belongs to the MenH-SHCHC complex in the closed conformation. The SHCHC ligand is represented in sticks with carbon and oxygen atoms colored in *yellow* and *red*, respectively. *Gray mesh* indicates electron density ($2F_o - F_c$) contoured at 1.5σ. The water molecule (*W*) is shown as a *red sphere*.

cally disfavored *gauche* conformation in the closed conformation (Fig. 3*E*). To accommodate these changes, Asp^{210} and His^{232} undergo a subtle positional movement of about 0.7 and 0.9 Å, respectively, in the closed conformation relative to the open conformation to finally form the functional catalytic triad (Fig. 3*E*). The positional change of Asp^{210} and His^{232} is a result of backbone shift in a large portion of the α/β-domain after the cap domain insertion, including αD, αE, αF′, αF, β7, and β8 (Fig. 3*C*).

The α/β-domain change causes abrupt and significant backbone change with a maximum displacement of more than 2.4 Å in the loop connecting αE to β8 (Fig. 3*C*), which includes residues 221–224 in the open conformation and residues 220–222 in the closed conformation. As a result, αE is shorter by one residue and β8 is longer by two residues in the closed conformation in comparison with the open conformation. In addition, Cys^{206} (in β7) and Cys^{224} are suitably positioned to form a disulfide bond in the open conformation but are too far apart to form a similar disulfide bond in the closed conformation. The disulfide bond would lock the enzyme in the inactive conformation and could be utilized to regulate MenH activity through a redox-responsive mechanism. However, the two cysteine res-

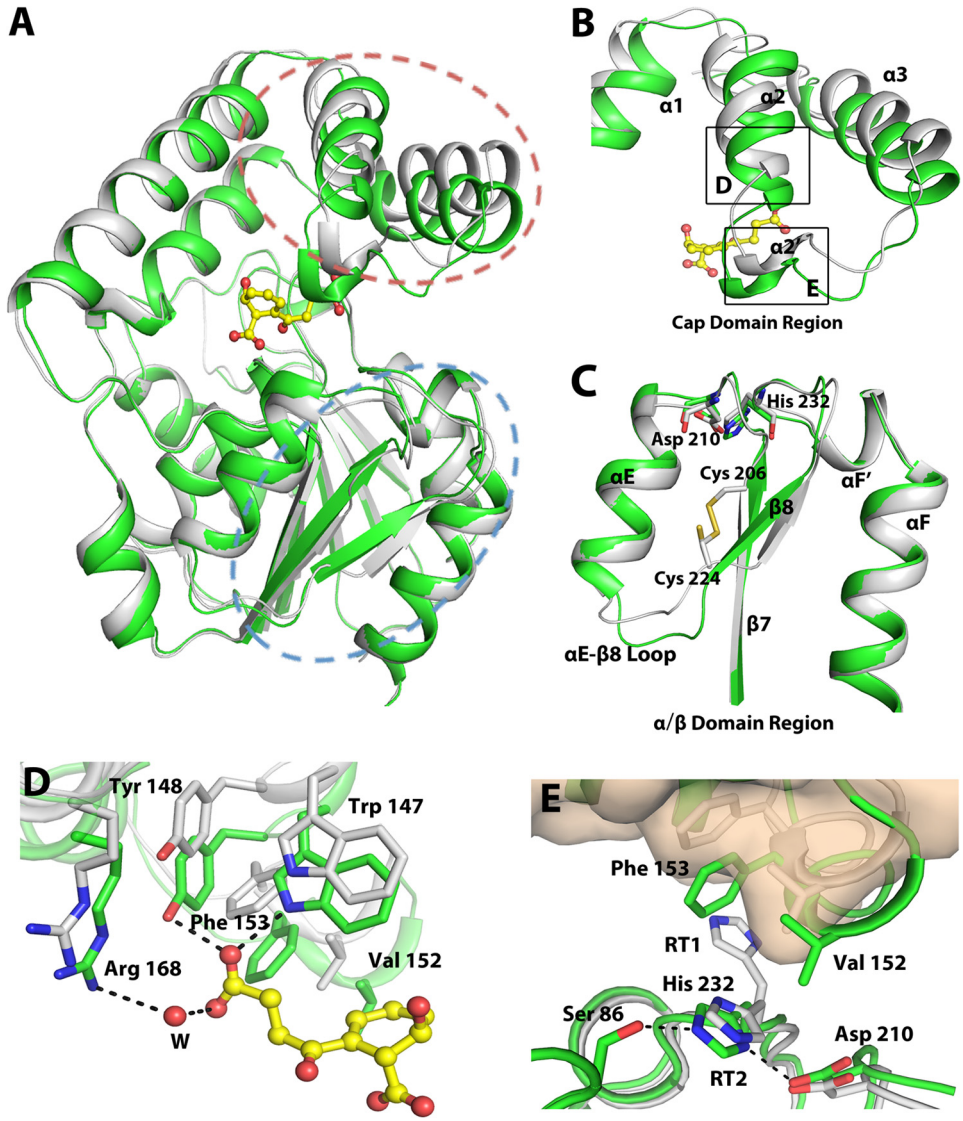

FIGURE 3. **Structural differences between the open and closed conformations.** *A*, superposition of the two structures. *B*, hinged movement of the α2- and α3-containing ensemble in the cap domain. *C*, large scale backbone movement in the α/β-domain. *D*, enzyme-SHCHC interactions enabled by the hinged movement. *E*, interaction of the α2′ 3_{10}-helix with the triad residues. The open ligand-free MenH structure is colored *gray*, and the closed MenH-SHCHC structure is colored *green* for all Cα atoms with their active site residues represented in sticks. *B* and *C* correspond to the regions *circled* in *broken red* and *blue lines* in *A*, respectively. The RT1 rotamer of His^{232} is omitted in *C*. *D* and *E* correspond to the *boxed* regions in *B*. In *E*, the α-helical cap domain of the open conformation is presented in *wheat* surface. *Dashed lines* indicate hydrogen bonds with a distance less than 3.5 Å. Water molecules (*W*) are shown as *red spheres*.

idues are not conserved among MenH orthologues. Their potential involvement in regulating the enzyme activity needs further investigation.

Enzyme-Ligand Interactions—The SHCHC product is bound firmly at identical position and orientation at the active sites of the binary and ternary complexes with a markedly lower B factor in comparison with other parts of the structures. Its average B factor is 12.8 $Å^2$ in the binary complex and 9.9 $Å^2$ in the ternary complex compared with an average B factor of 28.0 and 24.9 $Å^2$ for the protein (Table 1), respectively. The extensive interactions of this ligand with the enzyme include hydrophobic interactions with Trp^{147}, Val^{152}, and Phe^{153} (Fig. 3*D*); hydrogen bonding interactions with Tyr^{85}, Ser^{86}, Arg^{90}, Arg^{124}, Trp^{147}, Tyr^{148}, Arg^{168}, and Asn^{223}; and salt bridge interaction with Arg^{90} (Fig. 4). These interactions are consistent with findings in a previous mutational study (15), although the interaction with Arg^{168} is a water-mediated hydrogen bond rather than a salt bridge interaction. In addition, the product is also stabilized by two short hydrogen bonds provided by the backbone amides of Phe^{23} and Leu^{87} to the SHCHC succinyl keto group where an oxyanionic enolate intermediate is expected after α-proton abstraction in the MenH-catalyzed reaction. This finding strongly supports that the backbone amides of these residues or their equivalents in MenH orthologues form the oxyanion hole as proposed on the basis of modeling results (17, 18).

In the ternary complex, the pyruvate product is bound at a position close to the opening of the active site cavity to the bulk solvent. It is stabilized by only one hydrogen bond with the side-chain hydroxyl of Ser^{127} (Fig. 4*C*) and is close to the side-chain guanidinium group of Arg^{124} without direct interaction. This weak interaction suggests that pyruvate occupies a transient binding site on its exit from the active site after it is cleaved

TABLE 1
Data collection and refinement statistics
Values for the highest resolution shell are given in parentheses. N/A, not applicable.

	MenH	MenH-SHCHC	MenH-SHCHC-pyruvate
PDB code	4MXD	4MYD	4MYS
Data collection			
Space group	$P3_12_1$	$P3_1$	$P3_1$
Unit cell dimensions			
a, *b*, *c* (Å)	72.2, 72.2, 112.6	121.9, 121.9, 46.9	122.0, 122.0, 46.9
α, β, γ (°)	90, 90, 120	90, 90, 120	90, 90, 120
Redundancy	10.8 (10.9)	5.3 (4.9)	5.0 (4.6)
Completeness (%)	99.9 (100)	99.7 (99.7)	99.5 (97.4)
Reflections (unique)	656,511 (60,673)	855,411 (161,920)	729,480 (145,860)
I/σ_I	16.0 (5.3)	9.0 (2.3)	10.7 (2.9)
R_{merge}	0.091 (0.59)	0.083 (0.69)	0.090 (0.41)
Refinement			
Resolution range (Å)	50–1.45	46.8–1.37	37.2–1.42
No. of atoms	2,458	8,579	8,596
Macromolecules	2,069	7,748	7,724
Water	351	797	826
Ligands/ions	38	34	46
Average B factor (Å^2)	22.0	28.0	24.9
Macromolecules	19.5	23.2	21.4
Water	35.1	41.9	37.4
Ligand	N/A	12.2[a]	9.9/20.9[b]
R_{work}/R_{free} (%)	13.2/15.0	12.8/16.6	17.4/19.5
r.m.s.d. for ideal value			
Bond length (Å)	0.008	0.01	0.006
Bond angle (°)	1.30	1.20	1.08
Ramachandran plot			
Favored/allowed/outliers (%)	98.9/1.1/0	99.0/1.0/0	99.0/1/0

[a] Value for the SHCHC ligand.
[b] Values for SHCHC/pyruvate.

from the SEPHCHC substrate. Its close positioning to the Arg^{124} side chain is consistent with the suggestion that this residue is involved in the SEPHCHC substrate binding by forming a salt bridge with the pyruvyl carboxylate (15).

Site-directed Mutagenesis—In the closed conformation, Trp^{147} and Tyr^{148} strongly interact with the SHCHC ligand through both hydrogen bonding and hydrophobic interaction, whereas Val^{152} and Phe^{153} directly interact with the catalytic triad and force its formation. All these residues are highly conserved among MenH homologues (15, 18). To assess their catalytic contribution, the mutants V152A, V152G, F153A, Y148F, and Y148A were created. Two other single point mutants, W147A and W147F, were created and characterized in previous work (15). In addition, two double mutants, W147A/Y148A and V152G/F153A, were also constructed and expressed. The W147A/Y148A mutant presents a different circular dichroism spectrum compared with the wild-type enzyme, indicating that the protein structure is significantly altered. All other mutants were readily obtained in a stable and pure form with a CD spectrum closely similar to that of the wild-type enzyme.

The catalytic efficiency of V152A and F153A was reduced by 1230- and 11-fold (Table 2), respectively. When both residues were mutated, the catalytic activity was completely eliminated. To understand the meaning of these kinetic data, it is worth noting that Phe^{153}, despite its much lesser catalytic contribution, makes more hydrophobic contacts with the ligand than Val^{152} in the closed conformation (Fig. 3*D*). In addition, neither Val^{152} nor Phe^{153} makes a significant contribution to binding of the ligand compared with many other strong polar and nonpolar interactions (Fig. 4); however, they are essential to the catalysis as seen for the double mutant V152G/F153A. From these comparisons, it is clear that the catalytic contribution of Val^{152} and Phe^{153} is not limited to their contribution to the binding of substrate through hydrophobic interactions observed in the MenH-SHCHC complex (Fig. 3*D*); rather, their role in stabilizing and inducing the active closed conformation from the inactive conformation is likely a much more important catalytic contribution. Thus, the kinetic results of these mutants strongly support an essential role of the open-to-closed conformational change in MenH catalysis.

Both Trp^{147} and Tyr^{148} play an important role in the open-closed structural change by strongly interacting with the ligand through hydrogen bonding and hydrophobic interaction. This role is consistent with the kinetic properties of the proteins with a mutation at either position. As reported earlier (15), the catalytic efficiency of the W147A and W147F mutants is reduced by 5.9×10^3- and 62-fold, respectively. Similarly, mutation at the adjacent Tyr^{148} also caused a significant decrease in the second order rate constant (Table 2).

NMR Detection of the Catalytic Triad—It is well known that the hydrogen bond between the central histidine and the acidic residue (Asp or Glu) is strongly deshielded in the catalytic triads of serine proteases and α/β-hydrolase enzymes, affording a proton nuclear resonance signal in the downfield region (usually 12–16 ppm). When these enzymes interact with their mechanism-based inhibitors, the imidazole ring in the side chain of the central histidine is protonated, and its hydrogen bond with the acidic residue is greatly strengthened, leading to a significant downfield shift of the corresponding proton signal into the 16–19.5-ppm range (45–47). Based on these facts, we used NMR spectroscopy to detect the proton in the strong hydrogen bond between the side chains of Asp^{201} and His^{232} in the catalytic triad of ^{15}N-labeled MenH. As shown in Fig. 5, there is no signal in the 13–22-ppm range in the absence of a

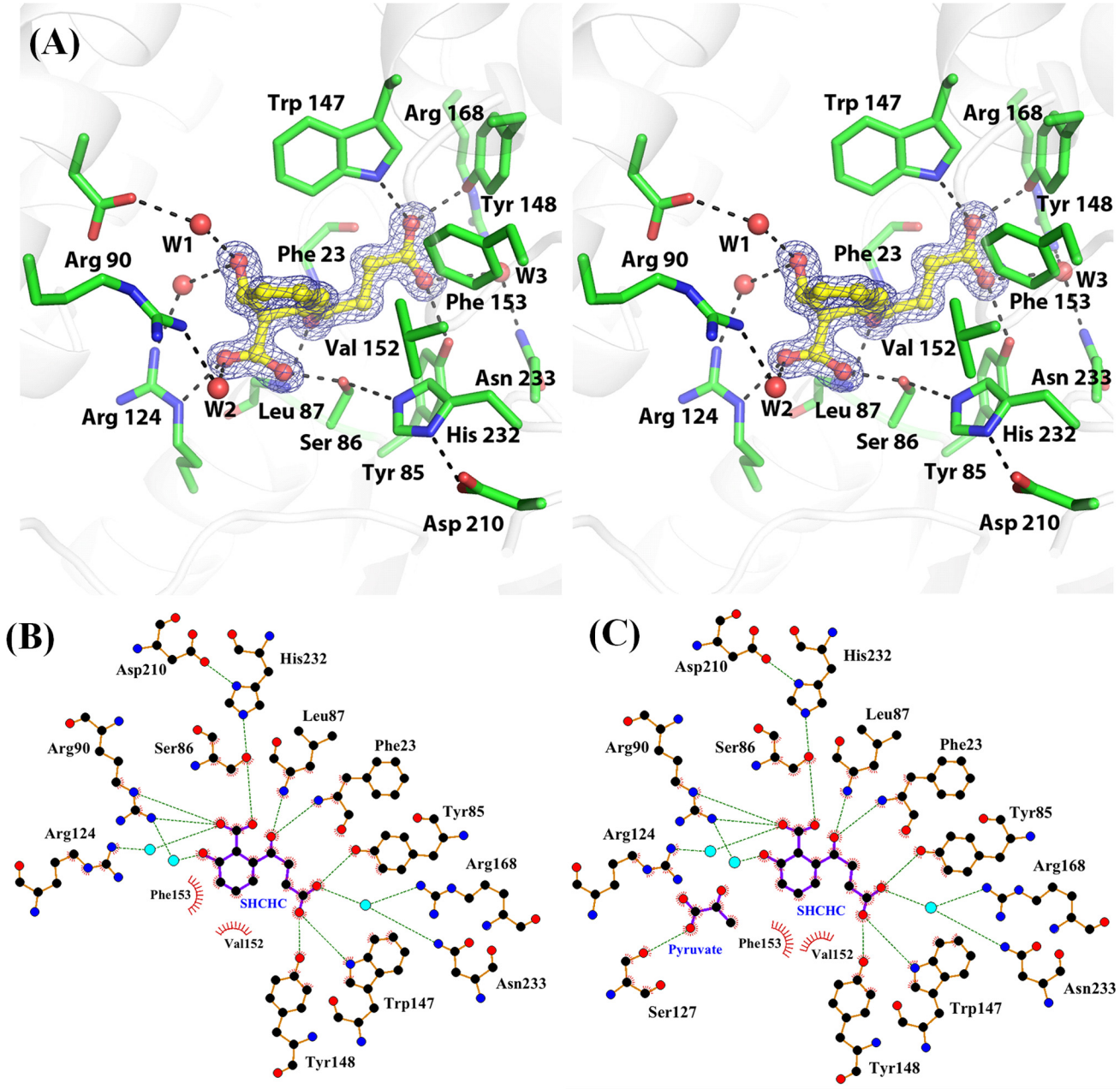

FIGURE 4. **Enzyme-ligand interactions.** *A*, stereodiagram of the active site of MenH in the binary MenH-SHCHC complex. The active site residues and the SHCHC are represented in sticks with *green* and *yellow* carbon atoms, respectively. Electron density ($2F_o - F_c$) of SHCHC is displayed in *blue mesh* and is contoured at 1.5σ. *B*, LIGPLOT of enzyme-ligand interactions in the binary MenH-SHCHC complex. *C*, LIGPLOT of enzyme-ligand interactions in the ternary MenH-SHCHC-pyruvate complex. *Dashed lines* indicate hydrogen bonds with a distance less than 3.5 Å. Water molecules (*W1–W3*) are shown as *red spheres*. The plots were generated with LIGPLOT V.4.5.3 (44).

TABLE 2
Kinetic constants of the E. coli MenH mutants

Protein	K_m	k_{cat}	k_{cat}/K_m
	μM	min^{-1}	$_M{}^{-1}\cdot min^{-1}$
Wild type	$(1.3 \pm 0.3) \times 10^1$	$(5.1 \pm 0.2) \times 10^2$	$(3.2 \pm 0.5) \times 10^7$
F153A	$(7 \pm 1) \times 10^1$	$(2.0 \pm 0.1) \times 10^2$	$(2.9 \pm 0.1) \times 10^6$
V152G	$(1.6 \pm 0.2) \times 10^2$	$(1.2 \pm 0.1) \times 10^1$	$(7.3 \pm 0.8) \times 10^4$
V152A	$(3.0 \pm 0.7) \times 10^2$	7.7 ± 0.9	$(2.6 \pm 0.2) \times 10^4$
Y148A	$(5.0 \pm 0.3) \times 10^1$	7.5 ± 0.8	$(1.6 \pm 0.3) \times 10^5$
Y148F	$(3.6 \pm 0.4) \times 10^1$	$(3.5 \pm 0.1) \times 10^1$	$(9.8 \pm 0.8) \times 10^5$
W147A/Y148A	ND[a]	ND	ND
V152G/F153A	ND	ND	ND

[a] ND, not detectable.

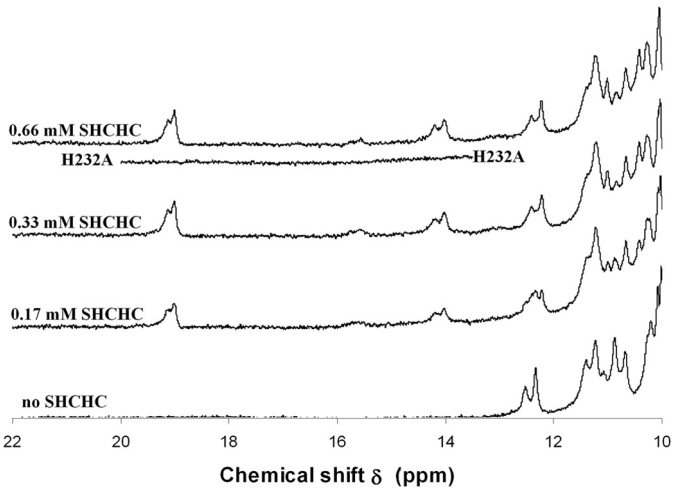

FIGURE 5. **^{1}H NMR spectra of MenH and its H232A mutant in the presence and absence of the SHCHC ligand.** The experiments were carried out in a solution containing 0.33 mM protein in 25 mM Tris-HCl, pH 8.0. The spectrum for the H232A mutant was obtained in the presence of 0.66 mM SHCHC.

ligand, whereas one broad peak at $\delta_H = 15.64$ ppm and two sets of bifurcated broad peaks centered at $\delta_H = 19.10$ and 14.16 ppm emerge with an increasing SHCHC concentration.

The proton signals at $\delta_H = 19.10$ and 14.16 ppm are split into doublets with a distance of 67 and 102 Hz, respectively, within the range of value for one-bond coupling with ^{15}N. In accordance with the empirical equations linking the hydrogen bond length to chemical shift (48, 49), they could originate from protons in N–H···O hydrogen bonds of 2.60 and 2.70 Å in aqueous solution that are close to the Asp^{210}-His^{232} hydrogen bond at 2.64 Å and the His^{232}-Ser^{86} hydrogen bond at 2.70 Å in the MenH-SHCHC crystal structure. Thus, these signals are believed to belong to the protons involved in the hydrogen bonds of the triad in the closed conformation. In support of this assignment, a similar bond length and proton chemical shift have been found for the two hydrogen bonds in the Ser-His-Asp triads of other enzymes (45–47, 50). Besides the two strong hydrogen bonds of the triad, there are two additional short hydrogen bonds between the SHCHC ligand and the side chains of Arg^{90} and Ser^{86} in the MenH-SHCHC structure that are 2.66 and 2.56 Å, respectively. Both protons in these additional strong hydrogen bonds are predicted to have a chemical shift of $\delta_H = 15.3$ ppm using the empirical equations (48, 49). Based on this prediction, these protons are believed to be responsible for the broad peak at $\delta_H = 15.64$ ppm that emerges after MenH binding of the SHCHC ligand.

The assignment of the signals at $\delta_H = 19.10$ and 14.16 ppm to the MenH catalytic triad is strongly supported by disappearance of the signals under the same conditions for the H232A mutant (Fig. 5), which is unable to form the triad but still binds the SHCHC ligand with an affinity ($K_D = 46 \pm 2$ μM) comparable with the wild-type enzyme ($K_D = 28 \pm 2$ μM) as determined by the SHCHC-dependent quenching of tryptophan fluorescence (Fig. 6). The absence of proton signals in the 13–22-ppm range for ligand-free MenH clearly demonstrates that the protein exists predominantly in the open conformation in solution and that the formation of its catalytic triad is totally dependent on a cognate ligand such as SHCHC. The fact that the crystal structures of the closed conformation were determined in the absence of ligands in previous investigations (Refs. 17 and 18 and Protein Data Bank code 1R3D) might be due to the better crystallizability of the closed structure in comparison with the open structure.

Fast Kinetics of Enzyme-Ligand Interactions—Fast kinetics of enzyme-ligand interactions were determined to understand the mechanism of MenH recognition of its substrate or other ligands. First, the stopped-flow technique was used to determine the pre-steady state kinetics of the MenH catalysis by monitoring formation of the SHCHC product, which was measured by the ultraviolet absorbance at 290 nm. No lag phase was detected in the product formation curves, and the calculated reaction rates were consistent with those obtained from the steady state measurements at various substrate concentrations. The absence of the lag phase strongly suggests that the substrate-induced open-closed structural change is much faster than the catalytic steps and is beyond the detection limit of the stopped-flow technique. Next, the MenH-SHCHC binding kinetics were determined by monitoring the quenching of tryptophan fluorescence at 340 nm, which is indicative of hydrogen bonding of the Trp^{147} side chain to SHCHC in the enzyme-ligand complex (Fig. 3*D*). As shown in Fig. 7, the observed rate of the approach to binding equilibrium k_{obs}, defined as the fluorescence quenching rate, increases hyperbolically with increasing ligand concentration. This positive hyperbolic k_{obs}-[SHCHC] relationship is predicted by an induced fit mechanism for the enzyme-ligand recognition under the rapid equilibrium approximation (51, 52). However, it is not unambiguous evidence for the induced fit mechanism. Actually, a conformational selection mechanism is also able to afford a similar rate-ligand concentration curve (53, 54), which has been demonstrated for several enzyme-ligand systems (53–56). Thus, the observed k_{obs}-[SHCHC] curve does not exclude a conformational selection mechanism for the MenH-ligand interaction.

DISCUSSION

The discovery of the inactive open conformation of MenH in its ligand-free form demonstrates the conformational flexibility of the α/β-hydrolase fold enzyme. Together with the active closed conformation determined previously (Ref. 17 and Protein Data Bank code 1R3D), this finding shows that the vitamin K biosynthetic enzyme is present in aqueous solution in one or both of the open and closed conformations. NMR evidence shows that MenH predominantly exists in the inactive open conformation in its ligand-free form, and it has to undergo a ligand-dependent open-closed conformational change in the catalytic process, similar to the structural change caused by the product ligand SHCHC. This open-closed structural change could occur via an induced fit mechanism (57) or a conformational selection mechanism (58). Unfortunately, neither the pre-steady state kinetics nor fast kinetic measurement of the MenH-SHCHC binding process provides an unambiguous distinction between these two possibilities. Nevertheless, the fact that the both open and closed conformations without a ligand have been readily crystallized indicates an equilibrium between them in solutions and strongly suggests that the conforma-

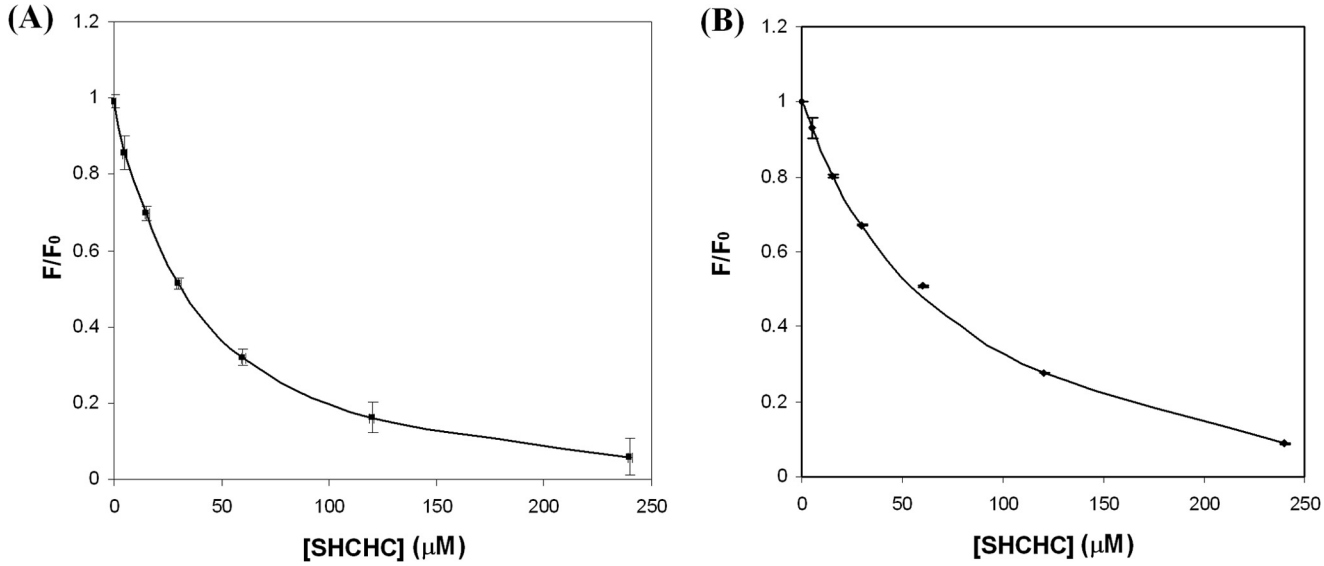

FIGURE 6. **Fluorometric determination of the SHCHC binding affinity of MenH and its H232A mutant.** *A*, titration curve for the wild-type MenH. *B*, titration curve for the H232A mutant. The tryptophan fluorescence (*F*) at 340 nm is normalized with the fluorescence emission of the protein (F_0) in the absence of the SHCHC ligand. The *solid lines* are the least square fitting results of the titration data.

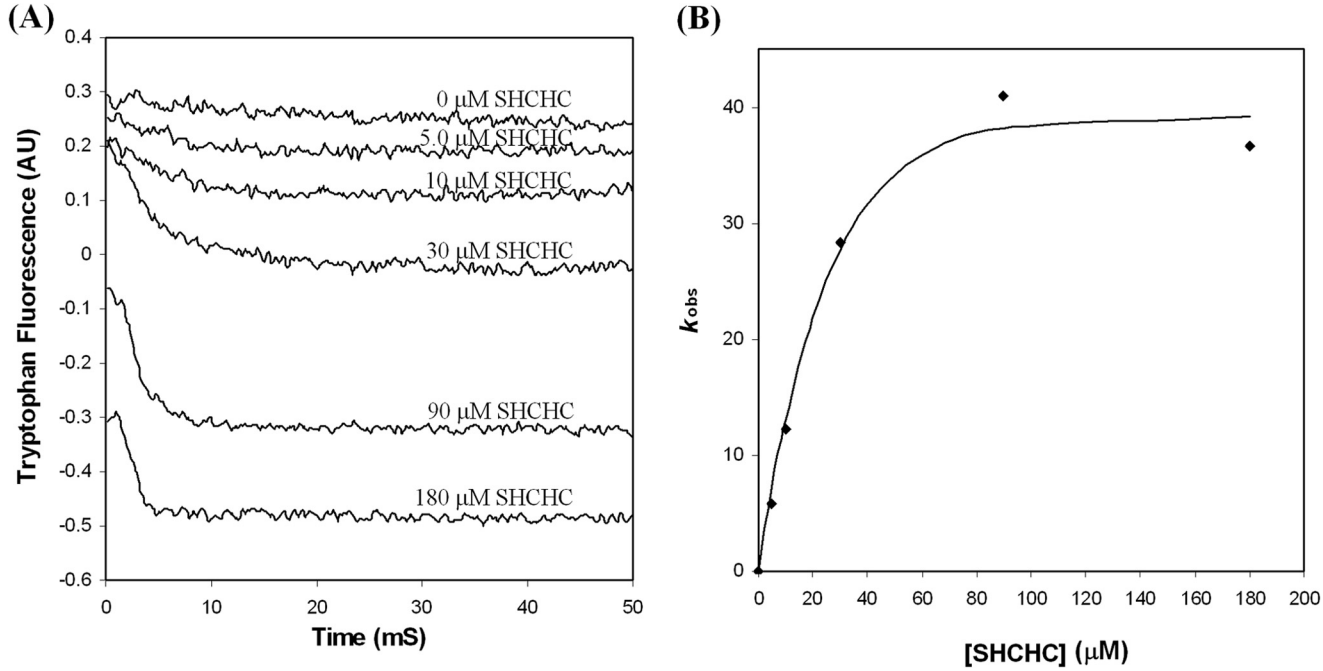

FIGURE 7. **Stop-flow measurement of the SHCHC binding by MenH.** *A*, the change of the MenH tryptophan fluorescence at 340 nm with time after mixing with SHCHC at varied concentrations. *B*, plot of the observed rate of the approach to binding equilibrium k_{obs} with the concentration of SHCHC. The *solid line* in *B* is the curve fitting result using a saturation growth model. *AU*, absorbance units.

tional change likely occurs via a conformational selection mechanism.

Results from the site-directed mutagenesis are consistent with an important catalytic role for the ligand-dependent open-closed conformational change (Table 2). This conformational change suggests a novel mechanism for modulating the intrinsic nucleophilic reactivity of the catalytic triad (Fig. 8). In the absence of a cognate ligand, the enzyme is in its dominant open conformation without a functional catalytic triad. The catalytic triad is formed and activated only when the substrate binds to the enzyme active site and stabilizes it in the active form. Such a triad may still retain its nucleophilicity but is unable to exhibit this reactivity because of the lack of a suitable electrophile in the enzyme-substrate complex. However, its basicity can be utilized to carry out the needed α-proton abstraction in the catalysis because the Oγ of Ser^{86} is optimally positioned for abstraction of a proton from C2 of the SEPHCHC substrate as suggested by its close distance of 2.3 Å from the C2 carbon of the SHCHC ligand and results from modeling of the substrate into the triad-containing structures of MenH (17, 18). In this way, the open-closed conformational change tightly couples formation of the catalytic triad to binding of the SEPHCHC substrate, thereby completely shielding the nucleophilicity of the triad and limiting its catalytic role to a specific general base.

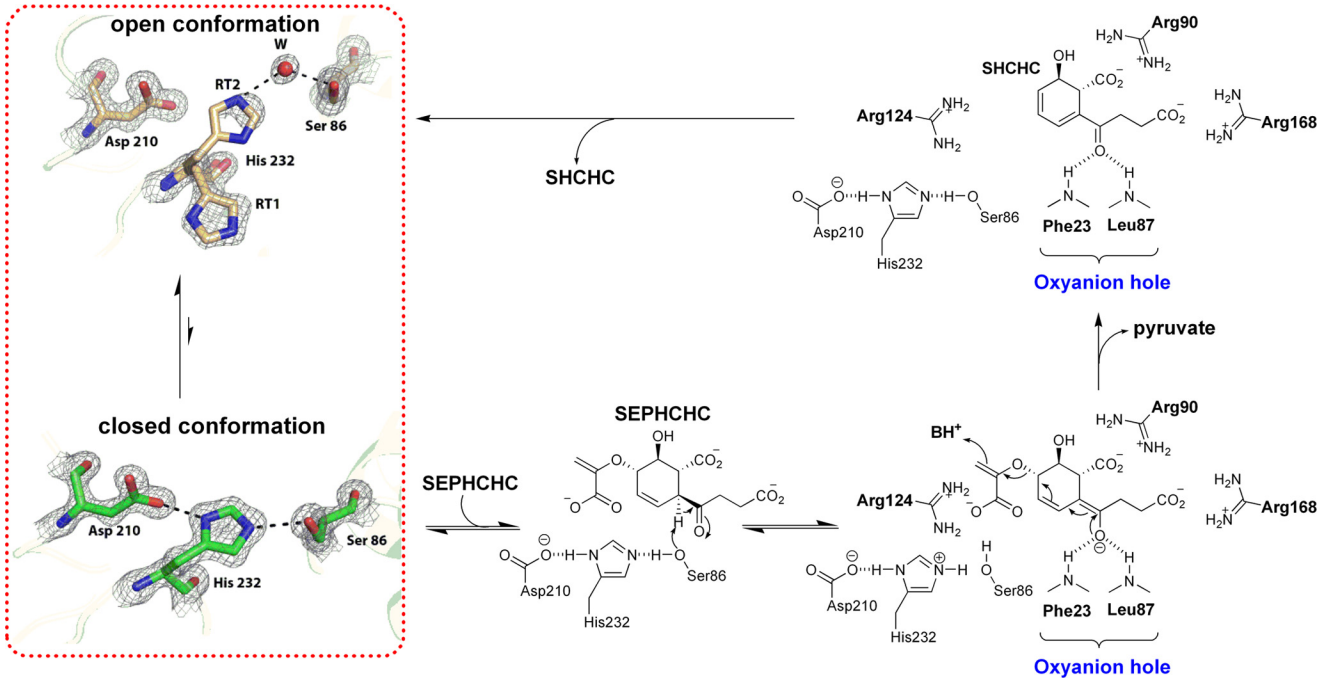

FIGURE 8. **Proposed catalytic mechanism of the MenH-catalyzed reaction.** This mechanism hypothesizes an open-closed conformational equilibrium (*circled* by the *dotted line*) that controls the reactivity of the Ser-His-Asp triad. Note that the enzyme-substrate interaction could also occur via an induced fit mechanism and that the interaction between Arg^{168} and the succinyl carboxylate of the intermediate or the SHCHC product is hydrogen bonding mediated by a water molecule (*W*) rather than a salt bridge.

This ligand-dependent triad formation also places a stringent constraint on the structure of the activating ligand and consequently greatly increases the substrate specificity of the enzyme, providing a rationale for its lack of hydrolytic activity toward nonnative esters or thioesters (14, 15).

With the modulation of the triad activity by the open-closed conformational change, a new catalytic mechanism is proposed for the MenH-catalyzed reaction as shown in Fig. 6. In this mechanism, MenH is stabilized in the active conformation after the negative SEPHCHC substrate is bound to the positively charged active site cavity through interactions with the conserved active site residues identified previously and in the current study. Subsequently, an oxyanion is generated via deprotonation of the Ser^{86} side-chain hydroxyl group by the Asp-His dyad to serve as a general base for abstraction of the C2 proton from the substrate. The resulting dienolate intermediate is stabilized by the oxyanion hole comprising the backbone amides of Phe^{23} and Leu^{87}. Next, the dienolate intermediate undergoes an E1cb elimination of the pyruvate to form the SHCHC product as proposed previously (15) using either water or the protonated side chain of Lys^{214} as the general acid to protonate the pyruvyl enolate. Finally, both products dissociate from the enzyme, and the protonated Asp-His dyad is deprotonated to transiently form the functional triad again. However, the triad then disintegrates after dissociation of the SHCHC product to complete a catalytic cycle.

The ligand-dependent conformational change is one of the most important features of the MenH catalysis. This type of conformational change, which usually involves local conformational change and no change of the catalytic triad, is well known to increase the substrate specificities and allosterically regulate the activities of serine proteases (4, 59, 60). In addition, conformational change is also known to play a critical role in the "interfacial activation" of lipases within the α/β-hydrolase superfamily that involves a low activity closed state in homogenous solution and a highly active open state when exposed to the substrate in an oil droplet. This structural change involves the movement of a long surface loop covering the active site in most lipases (61, 62) but involves an open-closed conformational change in the α-helical cap domain in other lipases (63, 64) that is similar to the changes observed for MenH. However, the interfacial activation of the lipases does not involve changes in the catalytic triad or the α/β-domain. In addition, the closed conformation of the lipases is inactive, which is opposite to what was observed for MenH. Thus, the open-closed conformational change of MenH is a novel, catalytically important structural change, which contributes to the structural and functional diversity of the α/β-hydrolase superfamily.

The ligand-dependent formation of the Ser-His-Asp triad is another important feature of the MenH catalysis that is rarely seen among triad-utilizing enzymes. Besides MenH, the serine protease Factor D in the alternative complement system is the only other enzyme that forms a functional triad after induction by substrate binding. In its resting state, Factor D also has a nonfunctional triad with the central histidine taking the energetically more favorable *trans* conformation and rotated out of the catalytic position due to the presence of a self-inhibitory loop (65). When its native substrate, a complex of the complement Factor C3b and Factor B, is bound, Factor D undergoes extensive conformational change to move the inhibitory loop and form the functional catalytic triad (16). Despite these similarities, the substrate induces conformation change to remove an obstacle to form the triad in Factor D from the three conserved residues that are thermodynamically favored to form the

triad, whereas the ligand-dependent conformational change in MenH forces the formation of the triad from three separated residues that are thermodynamically disfavored to form the catalytic motif. In addition, the Factor D catalytic triad still catalyzes the hydrolysis of C3b via the covalent, nucleophilic mechanism of catalysis like other serine proteases, whereas its reactivity is restricted to that of a general base in the MenH catalysis. Therefore, the ligand-dependent triad formation in MenH is a novel allosteric mechanism to modulate the reactivity of the catalytic triad, allowing the triad to expand its catalytic power beyond the covalent, nucleophilic catalysis.

In summary, we have found an open-closed conformational change critical to the catalysis of the α/β-hydrolase fold enzyme MenH that involves the formation of its Ser-His-Asp catalytic triad in the closed conformation and strictly subjects its enzymatic activity to control by the binding of a cognate ligand such as the substrate or the product. The coupling of the triad formation to the substrate binding shields the nucleophilicity of the traditional catalytic triad and effectively limits the triad to the role of a simple general base in the catalysis. Moreover, this control of the triad formation greatly increases the substrate specificities of the enzyme. These findings not only provide new insights into the catalytic mechanism of the typical α/β-hydrolase fold enzyme but also demonstrate that the traditional triad is capable of new catalytic chemistry through appropriate modulation.

Acknowledgments—We thank Nathaniel Echols, Pavel Afonine, Paul Adams, and Tom Terwilliger of the PHENIX team for help in solving the order-disorder structures.

REFERENCES

1. Page, M. J., and Di Cera, E. (2008) Serine peptidases: classification, structure and function. *Cell. Mol. Life Sci.* **65,** 1220–1236
2. Nardini, M., and Dijkstra, B. W. (1999) α/β Hydrolase fold enzymes: the family keeps growing. *Curr. Opin. Struct. Biol.* **9,** 732–737
3. Holmquist, M. (2000) α/β-Hydrolase fold enzymes: structures, functions and mechanisms. *Curr. Protein Pept. Sci.* **1,** 209–235
4. Hedstrom, L. (2002) Serine protease mechanism and specificity. *Chem. Rev.* **102,** 4501–4524
5. Wajant, H., and Pfizenmaier, K. (1996) Identification of potential active-site residues in the hydroxynitrile lyase from *Manihot esculenta* by site-directed mutagenesis. *J. Biol. Chem.* **271,** 25830–25834
6. Zuegg, J., Gruber, K., Gugganig, M., Wagner, U. G., and Kratky, C. (1999) Three-dimensional structures of enzyme-substrate complexes of the hydroxynitrile lyase from *Hevea brasiliensis*. *Protein Sci.* **8,** 1990–2000
7. Fleming, S. M., Robertson, T. A., Langley, G. J., and Bugg, T. D. (2000) Catalytic mechanism of a C–C hydrolase enzyme: evidence for a gem-diol intermediate, not an acyl enzyme. *Biochemistry* **39,** 1522–1531
8. Speare, D. M., Fleming, S. M., Beckett, M. N., Li, J. J., and Bugg, T. D. (2004) Synthetic 6-aryl-2-hydroxy-6-keto-hexa-2,4-dienoic acid substrates for C–C hydrolase BphD: investigation of a general base catalytic mechanism. *Org. Biomol. Chem.* **2,** 2942–2950
9. Li, J.-J., Li, C., Blindauer, C. A., and Bugg, T. D. (2006) Evidence for a *gem*-diol reaction intermediate in bacterial C–C hydrolase enzymes BphD and MhpC from ^{13}C NMR spectroscopy. *Biochemistry* **45,** 12461–12469
10. Ruzzini, A. C., Ghosh, S., Horsman, G. P., Foster, L. J., Bolin, J. T., and Eltis, L. D. (2012) Identification of an acyl-enzyme intermediate in a meta-cleavage product hydrolase reveals the versatility of the catalytic triad. *J. Am. Chem. Soc.* **134,** 4615–4624
11. Ruzzini, A. C., Horsman, G. P., and Eltis, L. D. (2012) The catalytic serine of MCP hydrolases is activated differently for C-O bond cleavage than for C-C bond cleavage. *Biochemistry* **51,** 5831–5840
12. Li, J.-J., and Bugg, T. D. H. (2007) Investigation of a general base mechanism for ester hydrolysis in C–C hydrolase enzymes of the α/β-hydrolase superfamily: a novel mechanism for the serine catalytic triad. *Org. Biomol. Chem.* **5,** 507–513
13. Wagner, U. G., Hasslacher, M., Griengl, H., Schwab, H., and Kratky, C. (1996) Mechanism of cyanogenesis: the crystal structure of hydroxynitrile lyase from *Hevea brasiliensis*. *Structure* **4,** 811–822
14. Jiang, M., Chen, X., Guo, Z.-F., Cao, Y., Chen, M., and Guo, Z. (2008) Identification and characterization of (1*R*,6*R*)-2-succinyl-6-hydroxy-2,4-cyclohexadiene-1-carboxylate synthase in the menaquinone biosynthesis of *Escherichia coli*. *Biochemistry* **47,** 3426–3434
15. Jiang, M., Chen, X., Wu, X.-H., Chen, M., Wu, Y. D., and Guo, Z. (2009) Catalytic mechanism of SHCHC synthase in the menaquinone biosynthesis of *Escherichia coli*: identification and mutational analysis of the active site residues. *Biochemistry* **48,** 6921–6931
16. Forneris, F., Ricklin, D., Wu, J., Tzekou, A., Wallace, R. S., Lambris, J. D., and Gros, P. (2010) Structure of C3b in complex with factors B and D give insight into complement convertase formation. *Science* **330,** 1816–1820
17. Dawson, A., Fyfe, P. K., Gillet, F., and Hunter, W. N. (2011) Exploiting the high-resolution crystal structure of *Staphylococcus aureus* MenH to gain insight into enzyme activity. *BMC Struct. Biol.* **11,** 19
18. Johnston, J. M., Jiang, M., Guo, Z., and Baker, E. N. (2013) Crystal structures of *E. coli* native MenH and two active site mutants. *PLoS One* **8,** e61325
19. Jiang, M., and Guo, Z. (2007) Effects of macromolecular crowding on the intrinsic catalytic efficiency and structure of enterobactin-specific isochorismate synthase. *J. Am. Chem. Soc.* **129,** 730–731
20. Guo, Z.-F., Jiang, M., Zheng, S., and Guo, Z. (2008) Suppression of linear side products by macromolecular crowding in nonribosomal enterobactin biosynthesis. *Org. Lett.* **10,** 649–652
21. Jiang, M., Cao, Y., Guo, Z.-F., Chen, M., Chen, X., and Guo, Z. (2007) Menaquinone biosynthesis in *Escherichia coli*: identification of 2-succinyl-5-enolpyruvyl-6-hydroxy-3-cyclohexene-1-carboxylate (SEPHCHC) as a novel intermediate and re-evaluation of MenD activity. *Biochemistry* **46,** 10979–10989
22. Jiang, M., Chen, M., Cao, Y., Yang, Y., Sze, K. H., Chen, X., and Guo, Z. (2007) Determination of the stereochemistry of 2-succinyl-5-enolpyruvyl-6-hydroxy-3-cyclohexene-1-carboxylic acid, a key intermediate in menaquinone biosynthesis. *Org. Lett.* **9,** 4765–4767
23. Grisostomi, G., Kast, P., Pulido, R., Huynh, J., and Hilvert, D. (1997) Efficient *in vivo* synthesis and rapid purification of chorismic acid using an engineered *Escherichia coli* strain. *Bioorg. Chem.* **25,** 297–305
24. Otwinowski, Z., and Minor, W. (1997) Processing of x-ray diffraction data collected in oscillation mode. *Methods Enzymol.* **276,** 307–326
25. McCoy, A. J., Grosse-Kunstleve, R. W., Adams, P. D., Winn, M. D., Storoni, L. C., and Read, R. J. (2007) Phaser crystallographic software. *J. Appl. Crystallogr.* **40,** 658–674
26. Collaborative Computational Project, Number 4 (1994) The CCP4 suite: programs for protein crystallography. *Acta Crystallogr. D Biol. Crystallogr.* **50,** 760–763
27. Langer, G., Cohen, S. X., Lamzin, V. S., and Perrakis, A. (2008) Automated macromolecular model building for x-ray crystallography using ARP/wARP version 7. *Nat. Protoc.* **3,** 1171–1179
28. Emsley, P., Lohkamp, B., Scott, W. G., and Cowtan, K. (2010) Features and development of Coot. *Acta Crystallogr. D Biol. Crystallogr.* **66,** 486–501
29. Vagin, A. A., Steiner, R. A., Lebedev, A. A., Potterton, L., McNicholas, S., Long, F., and Murshudov, G. N. (2004) REFMAC5 dictionary: organisation of prior chemical knowledge and guidelines for its use. *Acta Crystallogr. D Biol. Crystallogr.* **60,** 2184–2195
30. Adams, P. D., Afonine, P. V., Bunkóczi, G., Chen, V. B., Davis, I. W., Echols, N., Headd, J. J., Hung, L. W., Kapral, G. J., Grosse-Kunstleve, R. W., McCoy, A. J., Moriarty, N. W., Oeffner, R., Read, R. J., Richardson, D. C., Richardson, J. S., Terwilliger, T. C., and Zwart, P. H. (2010) PHENIX: a comprehensive Python-based system for macromolecular structure solution. *Acta Crystallogr. D Biol. Crystallogr.* **66,** 213–221
31. Laskowski, R. A., MacArthur, M. W., Moss, D. S., and Thornton, J. M. (1993) PROCHECK: a program to check the stereochemical quality of

protein structures. *J. Appl. Crystallogr.* **26,** 283–291
32. Chen, V. B., Arendall, W. B., 3rd, Headd, J. J., Keedy, D. A., Immormino, R. M., Kapral, G. J., Murray, L. W., Richardson, J. S., and Richardson, D. C. (2010) MolProbity: all-atom structure validation for macromolecular crystallography. *Acta Crystallogr. D Biol. Crystallogr.* **66,** 12–21
33. Long, F., Vagin, A. A., Young, P., and Murshudov, G. N. (2008) BALBES: a molecular replacement pipeline. *Acta Crystallogr. D Biol. Crystallogr.* **64,** 125–132
34. Zhang, T., Gu, Y.-X., Zheng, C.-D., and Fan, H.-F. (2010) OASIS4.0—a new version of the program OASIS for phasing protein diffraction data. *Chin. Phys. B* **19,** 086101
35. Hare, S., Cherepanov, P., and Wang, J. (2009) Application of general formulas for the correction of a lattice-translocation defect in crystals of a lentiviral integrase in complex with LEDGF. *Acta Crystallogr. D Biol. Crystallogr.* **65,** 966–973
36. Pletnev, S., Morozova, K. S., Verkhusha, V. V., and Dauter Z. (2009) Rotational order-disorder structure of fluorescent protein FP480. *Acta Crystallogr. D Biol. Crystallogr.* **65,** 906–912
37. Moriarty, N. W., Grosse-Kunstleve, R. W., and Adams, P. D. (2009) electronic Ligand Builder and Optimization Workbench (eLBOW): a tool for ligand coordinate and restraint generation. *Acta Crystallogr. D Biol. Crystallogr.* **65,** 1074–1080
38. Larkin, M. A., Blackshields, G., Brown, N. P., Chenna, R., McGettigan, P. A., McWilliam, H., Valentin, F., Wallace, I. M., Wilm, A., Lopez, R., Thompson, J. D., Gibson, T. J., Higgins, D. G. (2007) Clustal W and Clustal X version 2.0. *Bioinformatics* **23,** 2947–2948
39. DeLano, W. L. (2002) *The PyMOL Molecular Graphics System*, Schrödinger, LLC, New York
40. Krissinel, E., and Henrick, K. (2007) Inference of macromolecular assemblies from crystalline state. *J. Mol. Biol.* **372,** 774–797
41. Dundas, J., Ouyang, Z., Tseng, J., Binkowski, A., Turpaz, Y., and Liang, J. (2006) CASTp: computed atlas of surface topography of proteins with structural and topographical mapping of functionally annotated residues. *Nucleic Acids Res.* **34,** W116–W118
42. Ollis, D. L., Cheah, E., Cygler, M., Dijkstra, B., Frolow, F., Franken, S. M., Harel, M., Remington, S. J., Silman, I., Schrag, J., Sussman, J. L., Verschueren, K. H., and Goldman, A. (1992) The α/β hydrolase fold. *Protein Eng.* **5,** 197–211
43. Baker, N. A., Sept, D., Joseph, S., Holst, M. J., and McCammon, J. A. (2001) Electrostatics of nanosystems: application to microtubules and the ribosome. *Proc. Natl. Acad. Sci. U.S.A.* **98,** 10037–10041
44. Wallace, A. C., Laskowski, R. A., and Thornton, J. M. (1995) LIGPLOT: a program to generate schematic diagrams of protein-ligand interactions. *Protein Eng.* **8,** 127–134
45. Cassidy, C. S., Lin, J., and Frey, P. A. (1997) A new concept for the mechanism of action of chymotrypsin: the role of the low-barrier hydrogen bond. *Biochemistry* **36,** 4576–4584
46. Viragh, C., Harris, T. K., Reddy, P. M., Massiah, M. A., Mildvan, A. S., and Kovach, I. M. (2000) NMR evidence for a short, strong hydrogen bond at the active site of a cholinesterase. *Biochemistry* **39,** 16200–16205
47. Stranzl, G. R., Gruber, K., Steinkellner, G., Zangger, K., Schwab, H., and Kratky, C. (2004) Observation of a short, strong hydrogen bond in the active site of hydroxynitrile lyase from *Hevea brasiliensis*. *J. Biol. Chem.* **279,** 3699–3707
48. McDermott, A., Ridenour, C. F. (1996) in *Encyclopedia of NMR* (Grant, D. M., and Harris, R. K., eds), pp. 3820–3825, Wiley, Sussex, UK
49. Wei, Y., and McDermott, A. E. (1999) in *Modeling NMR Chemical Shifts: Gaining Insights into Structure and Environment* (Facelli, J. C., and de Dios, A. C., eds) pp. 177–193, Oxford University Press, Cary, NC
50. Harris, T. K., Mildvan, A. S. (1999) High-precision measurement of hydrogen bond lengths in proteins by nuclear magnetic resonance methods. *Proteins* **35,** 275–282
51. Tummino, P. J., and Copeland, R. A. (2008) Residence time of receptor-ligand complexes and its effect on biological function. *Biochemistry* **47,** 5481–5492
52. Johnson, K. A. (2008) Role of induced fit in enzyme specificity: a molecular forward/reverse switch. *J. Biol. Chem.* **283,** 26297–26301
53. Vogt, A. D., and Di Cera, E. (2012) Conformational selection or induced fit? A critical appraisal of the kinetic mechanism. *Biochemistry* **51,** 5894–5902
54. Vogt, A. D., and Di Cera, E. (2013) Conformational selection is a dominant mechanism of ligand binding. *Biochemistry* **52,** 5723–5729
55. Kim, Y. B., Kalinowski, S. S., and Marcinkeviciene, J. (2007) A presteady state analysis of ligand binding to human glucokinase: evidence for a preexisting equilibrium. *Biochemistry* **46,** 1423–1431
56. Antoine, M., Boutin, J. A., and Ferry, G. (2009) Binding kinetics of glucose and allosteric activators to human glucokinase reveal multiple conformational states. *Biochemistry* **48,** 5466–5482
57. Koshland, D. E., Jr., Némethy, G., and Filmer, D. (1966) Comparison of experimental binding data and theoretical models in proteins containing subunits. *Biochemistry* **5,** 365–385
58. Monod, J., Wyman, J., and Changeux, J. P. (1965) On the nature of allosteric transitions: a plausible model. *J. Mol. Biol.* **12,** 88–118
59. Perona, J. J., and Craik, C. S. (1995) Structural basis of substrate specificity in the serine proteases. *Protein Sci.* **4,** 337–360
60. Pozzi, N., Vogt, A. D., Gohara, D. W., and Di Cera, E. (2012) Conformational selection in trypsin-like proteases. *Curr. Opin. Struct. Biol.* **22,** 421–431
61. Brady, L., Brzozowski, A. M., Derewenda, Z. S., Dodson, E., Dodson, G., Tolley, S., Turkenburg, J. P., Christiansen, L., Huge-Jensen, B., Norskov, L., Thim, L., and Menge, U. (1990) A serine protease triad forms the catalytic centre of a triacylglycerol lipase. *Nature* **343,** 767–770
62. Brzozowski, A. M., Derewenda, U., Derewenda, Z. S., Dodson, G. G., Lawson, D. M., Turkenburg, J. P., Bjorkling, F., Huge-Jensen, B., Patkar, S. A., and Thim L. (1991) A model for interfacial activation in lipases from the structure of a fungal lipase-inhibitor complex. *Nature* **351,** 491–494
63. Schrag, J. D., Li, Y., Cygler, M., Lang, D., Burgdorf, T., Hecht, H. J., Schmid, R., Schomburg, D., Rydel, T. J., Oliver, J. D., Strickland, L. C., Dunaway, C. M., Larson, S. B., Day, J., and McPherson, A. (1997) The open conformation of a *Pseudomonas* lipase. *Structure* **5,** 187–202
64. Roussel, A., Canaan, S., Egloff, M.-P., Rivière, M., Dupuis, L., Verger, R., Cambillau, C. (1999) Crystal structure of human gastric lipase and model of lysosomal acid lipase, two lipolytic enzymes of medical interest. *J. Biol. Chem.* **274,** 16995–17002
65. Narayana, S. V., Carson, M., el-Kabbani, O., Kilpatrick, J. M., Moore, D., Chen, X., Bugg, C. E., Volanakis, J. E., and DeLucas, L. J. (1994) Structure of human factor D. A complement system protein at 2.0 Å resolution. *J. Mol. Biol.* **235,** 695–708